

# Adapter Merging with Centroid Prototype Mapping for Scalable Class-Incremental Learning

Takuma Fukuda<sup>1</sup>Hiroshi Kera<sup>2</sup>Kazuhiko Kawamoto<sup>3</sup>

Chiba University

<sup>1</sup>takuma.fukuda@chiba-u.jp, <sup>2</sup>kera@chiba-u.jp, <sup>3</sup>kawa@faculty.chiba-u.jp

## Abstract

We propose *Adapter Merging with Centroid Prototype Mapping (ACMap)*, an exemplar-free framework for class-incremental learning (CIL) that addresses both catastrophic forgetting and scalability. While existing methods trade-off between inference time and accuracy, ACMap consolidates task-specific adapters into a single adapter, ensuring constant inference time across tasks without compromising accuracy. The framework employs adapter merging to build a shared subspace that aligns task representations and mitigates forgetting, while centroid prototype mapping maintains high accuracy through consistent adaptation in the shared subspace. To further improve scalability, an early stopping strategy limits adapter merging as tasks increase. Extensive experiments on five benchmark datasets demonstrate that ACMap matches state-of-the-art accuracy while maintaining inference time comparable to the fastest existing methods. The code is available at <https://github.com/tf63/ACMap>.

## 1. Introduction

In real-world applications, data often arrives sequentially, which requires continual learning [41] to adapt to evolving data distributions. Class-incremental learning (CIL) [33] is a branch of continual learning designed for scenarios where tasks with new classes appear sequentially. A primary challenge in CIL is, known as *catastrophic forgetting* [10], to learn new tasks while preserving knowledge from previous ones. Traditional CIL methods mitigate catastrophic forgetting by retaining representative data (exemplars) from previous tasks [3, 28, 35] or by dynamically adjusting network structures [46, 52, 54]. However, privacy concerns [36] often limit the use of exemplars. This limitation highlights the need for exemplar-free methods in practical applications.

In contrast to traditional approaches, recent CIL methods [55] based on pre-trained models have attracted attention. These methods aim to mitigate catastrophic for-

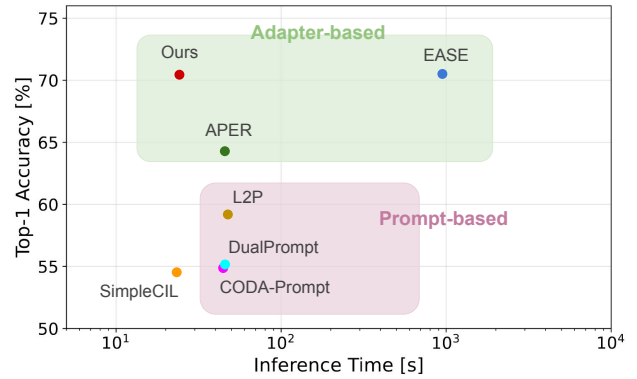


Figure 1. Comparison of the final top-1 accuracy and inference time for task 40 of ImageNet-R in class-incremental learning. The comparison includes L2P [48], DualPrompt [47], CODA-Prompt [38], SimpleCIL [58], APER [58], EASE [56], and our method. All methods use the same backbone (ViT-B/16). Our method performs well in terms of both inference time and accuracy by consolidating task-specific adapters into a single adapter.

getting by leveraging the robust generalization capabilities of pre-trained models. Typically, these methods incorporate parameter-efficient modules for task-specific training on each CIL task, such as prompts [21] or adapters [31]. While effective for domain adaptation, task-specific classifiers often encounter scalability limitations during inference. Figure 1 compares the final top-1 accuracy and inference time on task 40 of ImageNet-R in CIL for these methods. The results demonstrate a trade-off between accuracy and inference time. This trade-off indicates the challenge of achieving both high accuracy and scalability at inference.

To address the dual challenges of catastrophic forgetting and scalability in CIL, we propose **Adapter Merging with Centroid Prototype Mapping (ACMap)**, a framework that consolidates task-specific adapters into a single adapter. ACMap achieves constant inference time as the number of tasks increases, providing scalability without sacrificing accuracy. Furthermore, ACMap’s exemplar-free design ad-

dresses privacy concerns commonly associated with traditional exemplar-based methods.

ACMap comprises two core components: adapter merging and centroid prototype mapping. Adapter merging incrementally combines task-specific adapters into a shared subspace by averaging their weights. This shared subspace mitigates catastrophic forgetting by aligning tasks within the parameter space. While simple weight averaging alone may not ensure optimal performance, ACMap enhances alignment by initializing each adapter from a common starting weight. This initialization promotes similar training paths across tasks, encouraging the formation of a low-loss basin in the parameter space. Centroid prototype mapping further supports ACMap’s effectiveness by preserving previously learned representations through consistent adaptation across the shared subspace. To further improve scalability, an early stopping strategy reduces computational demands for training by limiting adapter merging. Evaluations on five benchmark datasets demonstrate that ACMap achieves state-of-the-art accuracy and efficient inference simultaneously. Specifically, on task 40 of ImageNet-R, ACMap improves final accuracy by more than 16% compared to the fastest existing method with similar inference speed while achieving a 39-fold inference speedup over the state-of-the-art method with comparable accuracy (see Figure 1).

In summary, our contributions are as follows:

1. We propose ACMap, a continual learning framework that consolidates task-specific adapters into a single shared subspace without storing previous data samples, effectively mitigating catastrophic forgetting.
2. To preserve previously learned representations, we incorporate centroid prototype mapping, ensuring consistency across tasks through adaptive subspace alignment.
3. Extensive experiments on five benchmark datasets demonstrate that ACMap achieves state-of-the-art accuracy and the fastest inference speed, validating its effectiveness and scalability in real-world applications.

## 2. Related Work

This section discusses traditional class-incremental learning methods and recent approaches with pre-trained models.

**Class-Incremental Learning (CIL).** Class-incremental learning (CIL) [57] is a learning paradigm in which a model incrementally learns new class information without forgetting previously learned classes. A major challenge in CIL is *catastrophic forgetting* [10, 22], where learning new classes overwrites information from older classes. This often results in significant performance degradation on earlier tasks. To address catastrophic forgetting, prior research can be broadly categorized into three main approaches [57]. The first approach [3, 4, 27, 28, 30, 35, 42] selects and retains

representative data (*exemplars*) from previously learned classes. The second approach [2, 9, 32, 46, 52, 54] dynamically modifies the model architecture to accommodate new class information. The third approach [6, 8, 19, 26, 33, 37] leverages knowledge distillation [17] to transfer knowledge from previously learned classes. However, even with these methods, catastrophic forgetting still leads to significant performance degradation. Additionally, many of these approaches rely on the use of exemplars, which can pose challenges related to privacy or storage constraints [57]. Therefore, unresolved issues remain for real-world applications.

**CIL with Pre-Trained Models.** Recently, there has been growing interest in utilizing large-scale pre-trained models for CIL [13, 55]. In these studies, parameter-efficient modules [14] are commonly employed to learn new tasks while preserving the strong generalization capabilities of the pre-trained model. Two primary approaches have emerged: (i) using learnable parameters (*prompts*) [21] concatenated to input vectors in pre-trained models, and (ii) incorporating adapter modules (e.g., LoRA [18]) into pre-trained models. s are exemplar-free and demonstrate significantly improved performance over approaches without pre-trained models. exemplar-free methods

**Adapter-based Approaches.** The second approach utilizes parameter-efficient adapter modules, such as LoRA. SimpleCIL [58] is a foundational method that constructs a cosine classifier [11] from the average of class-specific feature vector (*prototype*) [39] extracted from a pre-trained model using validation datasets. Although straightforward, SimpleCIL is comparable to methods based on VPT. APER [58] builds on SimpleCIL by using a pre-trained model with an adapter learned from the first task. EASE [56] achieves state-of-the-art performance by using task-specific adapters to extract prototypes for each task and constructing a cosine classifier from the concatenated prototypes. In an exemplar-free setting, where prototypes from previous classes cannot be extracted, EASE complements them through cosine similarity-based mapping. While APER has limited domain adaptation capabilities due to training an adapter only for the first task, EASE exhibits high adaptability by training adapters for all tasks. However, EASE incurs higher inference costs as the number of tasks grows, since feature vectors are extracted using each adapter individually. To address this lack of scalability, our method consolidates multiple adapters into a single one through adapter merging.

## 3. Preliminaries

This section introduces the problem formulation of CIL and provides the background on CIL approaches with pre-

trained models.

### 3.1. Problem Setting

**Class-Incremental Learning:** Class-incremental learning is a learning paradigm where a model is required to sequentially learn a series of  $T$  task datasets,  $\mathcal{D}_1, \dots, \mathcal{D}_T$ , while retaining knowledge of previously learned tasks. Each dataset  $\mathcal{D}_t = \{(\mathbf{x}_t, y_t)\}$  consists of pairs of input data  $\mathbf{x}_t \in \mathcal{X}$  and corresponding class label  $y_t \in \mathcal{Y}_t$ .<sup>1</sup> For any two distinct tasks  $t$  and  $t'$ , the class sets are disjoint, i.e.,  $\mathcal{Y}_t \cap \mathcal{Y}_{t'} = \emptyset$ . The objective in the  $t$ -th task is to learn a model  $f_\theta : \mathcal{X} \rightarrow \mathcal{Y}_t$ , parameterized by  $\theta$ , that accurately maps inputs to their class labels. During testing on  $t$ -th task, the model is evaluated on the cumulative test dataset  $\mathcal{T}_1 \cup \dots \cup \mathcal{T}_t$ , where  $\mathcal{T}_i$  is the test dataset for the  $i$ -th task.

**Exemplar & Exemplar-Free CIL:** Many traditional CIL approaches retain a subset of representative data from previous tasks, known as an exemplar set. This set for the  $t$ -th task is denoted  $\mathcal{E}_t = \{(\mathbf{x}^e, y^e)\}$ . In exemplar-based CIL, the training dataset for  $f_\theta$  includes both  $\mathcal{D}_t$  and exemplars from previous tasks, combined as  $\mathcal{D}_t \cup \mathcal{E}_1 \cup \dots \cup \mathcal{E}_t$ . However, privacy concerns and other constraints in real-world applications often restrict the use of exemplars. In exemplar-free settings,  $f_\theta$  is trained exclusively on the current task dataset  $\mathcal{D}_t$ . This study evaluates our approach under exemplar-free conditions to ensure broader applicability in privacy-sensitive scenarios.

### 3.2. Pre-Trained Models for CIL

Following previous studies [56, 58], we utilize a pre-trained Vision Transformer (ViT) [7, 44] to initialize  $f$ . The model is decomposed into a linear classifier  $\mathbf{W} \in \mathbb{R}^{d \times |\mathcal{Y}_t|}$  and a feature embedding function  $\phi : \mathbb{R}^D \rightarrow \mathbb{R}^d$ , where  $D$  is the dimension of the input vector and  $d$  is the embedding dimension. The function  $\phi$  denotes the final [CLS] token embedding in ViT, which represents the global image feature. For an input  $\mathbf{x} \in \mathbb{R}^D$ , the model output is given by  $f(\mathbf{x}) = \mathbf{W}^T \phi(\mathbf{x})$ .

**Adapter-based CIL:** Trainable parameter-efficient adapter modules are often employed when applying a pre-trained model to a task. The adapter has a bottleneck structure, consisting of a down-projection layer  $\mathbf{W}_{\text{down}} \in \mathbb{R}^{d \times r}$  and an up-projection layer  $\mathbf{W}_{\text{up}} \in \mathbb{R}^{r \times d}$ , where  $r$  is the bottleneck dimension and satisfies  $r \ll d$ . To introduce non-linearity, a ReLU layer is positioned between the projection layers. The adapter is connected to the MLP layer via a residual connection. Given the input of the MLP layer as  $\mathbf{x}_{\text{in}} \in \mathbb{R}^{d \times d}$ , the modified output  $\mathbf{x}_{\text{out}} \in \mathbb{R}^{d \times d}$  with

<sup>1</sup>We drop the index  $i$  from  $(\mathbf{x}_{t,i}, y_{t,i})$  for notational simplicity.

the adapter becomes:

$$\mathbf{x}_{\text{out}} = \text{MLP}(\mathbf{x}_{\text{in}}) + \text{ReLU}(\mathbf{x}_{\text{in}} \mathbf{W}_{\text{down}}) \mathbf{W}_{\text{up}}. \quad (1)$$

The adapter is inserted across each  $N_{\text{blocks}}$  transformer blocks. From this point onward, we will refer to the set of these  $N_{\text{blocks}}$  adapters collectively as “the adapter”, denoted as  $\mathcal{A}$ . In adapter-based CIL, a task-specific subspace is formed by training an adapter  $\mathcal{A}_t$  for each task  $t$ .

**Prototypical Classification in CIL:** After training the adapter on the  $t$ -th task, a prototypical classifier is constructed using the  $t$ -th validation dataset  $\mathcal{V}_t$ . Specifically, we calculate the prototype  $\mathbf{p}_{t,c} \in \mathbb{R}^d$ , which is the mean of the feature vectors for each class  $c \in \mathcal{Y}_t$ , as follows:

$$\mathbf{p}_{t,c} = \sum_{(\mathbf{x}_t, y_t) \in \mathcal{V}_t} \phi(\mathbf{x}_t) \mathbb{I}(y_t = c), \quad (2)$$

where  $\mathbb{I}(\cdot)$  is the indicator function. Then, the prototypes are concatenated to define the prototype matrix  $\mathbf{P}_t \in \mathbb{R}^{C_t \times d}$ , where  $C_t = |\mathcal{Y}_t|$  and

$$\mathbf{P}_t = [\mathbf{p}_{t,1} \quad \dots \quad \mathbf{p}_{t,C_t}]. \quad (3)$$

This calculation is performed within  $\mathcal{A}_1$ 's subspace [58] or across all subspaces [56]. During inference, the prototype matrices are used as the classifier weights  $\mathbf{W} = [\mathbf{P}_1 \quad \dots \quad \mathbf{P}_t] \in \mathbb{R}^{C \times d}$ , where  $C$  is the total number of classes  $\sum_{i=1}^t C_i$  learned so far. The model output  $f$  is redefined with a cosine classifier [11] as follows:

$$f(\mathbf{x}) = \frac{\mathbf{W}^T \phi(\mathbf{x})}{\|\mathbf{W}\|_2 \|\phi(\mathbf{x})\|_2}, \quad (4)$$

where  $\|\cdot\|_2$  denotes the  $\ell_2$ -norm. The predicted class of  $\mathbf{x}$  is determined as the class with the highest cosine similarity among the elements of  $f(\mathbf{x})$ . Note that the prototypes of previous classes are not included in  $\mathcal{V}_t$  and, therefore, cannot be calculated. In other words, in  $\mathcal{A}_t$ 's subspace, it is impossible to calculate  $\mathbf{P}_1, \dots, \mathbf{P}_{t-1}$ . These prototypes must be complemented with appropriate alignments.

## 4. ACMap: Adapter Merging with Centroid Prototype Mapping

In this paper, we propose Adapter Merging with Centroid Prototype Mapping (ACMap) for scalable CIL. Existing methods that rely on task-specific training for CIL often struggle with scalability during inference. ACMap addresses this challenge by training task-specific adapters and then consolidating them into a single unified adapter through a process called *adapter merging*. This approach allows ACMap to maintain scalability, requiring only the merged adapter during inference, while ensuring efficiency as tasks increase.

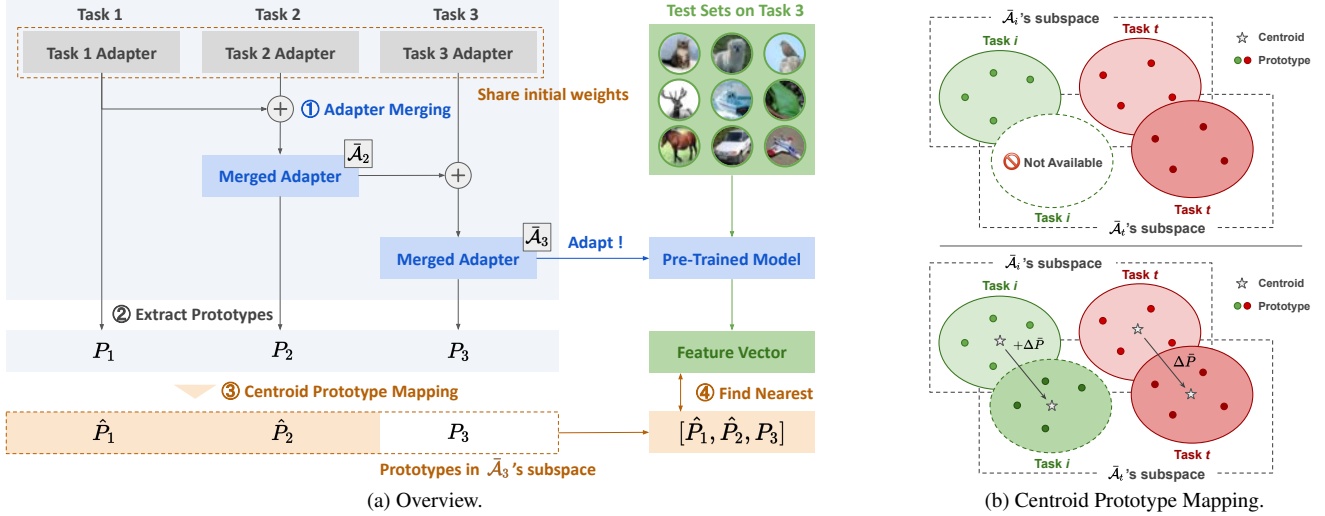


Figure 2. An Illustration of ACMAP. ACMAP sequentially trains an adapter for each task, starting from shared initial weights and incrementally merging them into a single adapter. In the subspace formed by the merged adapter, the prototypes for the current task are computed, while previous prototypes are updated via centroid prototype mapping.

#### 4.1. Adapter Merging in CIL

As illustrated in Figure 2a, ACMAP follows a sequential process where a task-specific adapter is trained for each task, and the merged adapter  $\bar{\mathcal{A}}$  is incrementally updated via adapter merging.

**Adapter Merging:** Adapter merging is a model merging technique that combines multiple adapters, inspired by previous work on model merging [20, 29, 50, 51]. A common approach for model merging is average merging [50], which averages the weights of multiple models with a shared initial weight. In ACMAP, each task-specific adapter starts with shared initial weights  $\theta_{\text{init}}$  and undergoes task-specific training to update the weights  $\theta_t$  for each task. The merged adapter is initialized as  $\bar{\mathcal{A}}_1 = \mathcal{A}_1$ , and its weights  $\bar{\theta}_t$  are iteratively updated using average merging as follows:

$$\bar{\theta}_t = \left(1 - \frac{1}{t}\right) \bar{\theta}_{t-1} + \frac{1}{t} \theta_t, \quad t = 2, \dots, T. \quad (5)$$

Through this process, the adapter  $\bar{\mathcal{A}}_t$  constructs a task-shared subspace that integrates the knowledge from all previous tasks. Weight averaging generally enhances both accuracy and robustness to distribution shifts compared to using a single model [24].

**Towards Effective Weight Averaging:** However, simply averaging the weights of different models does not guarantee optimal performance, particularly without proper alignment [1, 24, 25, 40]. For weight averaging to be effective, models should ideally originate from a common pre-

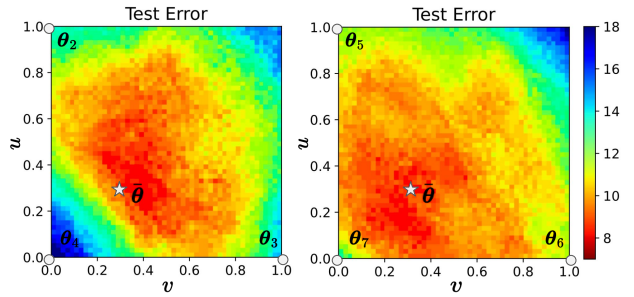


Figure 3. Visualization of the test error using linearly interpolated adapter weights  $\theta = u\theta_{t-1} + v\theta_t + (1-u-v)\theta_{t+1}$ , ( $0 \leq u, v \leq 1$ ) across three consecutive adapter weights  $\theta_{t-1}, \theta_t, \theta_{t+1}$ . Test errors for the adapters  $\theta_2, \theta_3, \theta_4$  are shown on the left, and for the adapters  $\theta_5, \theta_6, \theta_7$  on the right. The star symbol indicates the average merging ( $u = 1/3, v = 1/3$ ). Additional results are provided in Appendix D.2.

trained model or be fine-tuned in a similar region of parameter space. This alignment helps reduce variance, enhances regularization, and ensures that interpolated weights remain within a low-loss basin, thereby supporting stable and improved performance [24].

**Landscape Analysis for Adapter Merging:** We analyze the loss landscape of three successive adapters, as shown in Figure 3, through the linear interpolation  $\theta = u\theta_{t-1} + v\theta_t + (1-u-v)\theta_{t+1}$ , ( $0 \leq u, v \leq 1$ ), where  $\theta_{t-1}, \theta_t$ , and  $\theta_{t+1}$  represent the adapters trained on tasks  $t-1, t$ , and  $t+1$ , respectively. The test dataset is a combination of all three tasks:  $\mathcal{T}_{t-1} \cup \mathcal{T}_t \cup \mathcal{T}_{t+1}$ . This analysis shows the ex-



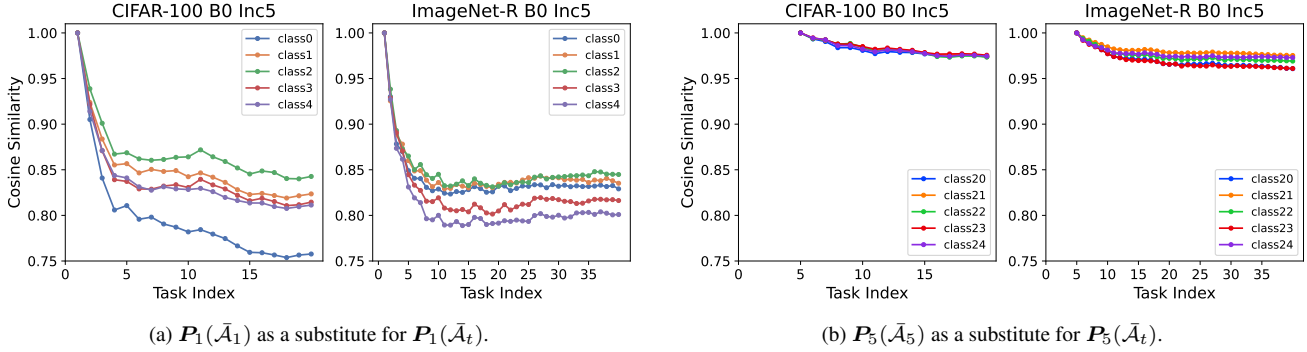


Figure 4. The curve showing the differences in cosine similarity that arise when earlier task prototypes are substituted for prototypes in subsequent subspaces.

istence of a low-loss basin (red region), indicating that the interpolated weights exhibit consistent performance across the tasks. This basin likely arises because each adapter is initialized with the same starting parameter. This initialization leads to similar training paths in the parameter space and helps form a shared low-loss region.

**Initial Weight Replacement:** To further encourage the formation of a low-loss basin, we propose *initial weight replacement*. After training on the first task, a shared initial weight  $\theta_{\text{init}}$ , which is typically initialized randomly, is replaced with  $\theta_1$ , the parameters learned from the first task. Hence, adapters for subsequent tasks  $i$  ( $> 1$ ) are trained with  $\theta_1$  as its initial parameter. By sharing the weight of the first adapter, subsequent tasks are more likely to follow similar training paths, helping convergence within a shared low-loss region.

## 4.2. Prototype Mapping

In ACMMap, a key challenge is an inability to compute previous prototypes within the subspace of the current adapter  $\bar{\mathcal{A}}_t$ , due to restricted access to data from previous tasks. Specifically, for task  $t$ , previous prototypes  $P_i(\bar{\mathcal{A}}_t)$ ,  $i = 1, \dots, t-1$  cannot be computed within the current subspace, where  $P_i(\bar{\mathcal{A}}_t)$  denotes the prototypes for task  $i$  computed using the current adapter  $\bar{\mathcal{A}}_t$ . This limitation arises because, in the CIL setting, data from previous tasks is unavailable, as shown in Figure 2b (top).

While the unavailable prototypes can be substituted with  $P_i(\bar{\mathcal{A}}_i)$ ,  $i = 1, \dots, t-1$  from previous subspaces, such substitutions may lead to an alignment problem. Figure 4a shows the cosine similarity  $\text{Sim}(P_1(\bar{\mathcal{A}}_1), P_1(\bar{\mathcal{A}}_t))$  when substituting  $P_1(\bar{\mathcal{A}}_1)$  for  $P_1(\bar{\mathcal{A}}_t)$  where  $\text{Sim}(\cdot, \cdot)$  denotes cosine similarity. This result shows that earlier task prototypes, such as from  $t = 1$ , shift significantly when applied to later subspaces, indicating poor alignment. Therefore, aligning prototypes within the current adapter is crucial for

accurate and consistent prototype mapping.

In contrast, Figure 4b shows using  $P_5(\bar{\mathcal{A}}_5)$  as a substitute for  $P_5(\bar{\mathcal{A}}_t)$  maintains high cosine similarities. This suggests that the alignment problem is not as severe. We will discuss this at the end of this section.

**Centroid Prototype Mapping:** The above alignment problem can be formulated as finding a mapping  $f$ :  $P_i(\bar{\mathcal{A}}_t) = f(P_i(\bar{\mathcal{A}}_i))$ ,  $i = 1, \dots, t-1$ . However, since the mapping  $f$  is generally unknown, we approximate it with an affine mapping:

$$P_i(\bar{\mathcal{A}}_t) \approx P_i(\bar{\mathcal{A}}_i) + \Delta P. \quad (6)$$

We estimate  $\Delta P$  as the difference between the centroids of the available prototypes  $P_t(\bar{\mathcal{A}}_t)$  and  $P_t(\bar{\mathcal{A}}_i)$ , i.e.,

$$\Delta P = \mathbb{E}[P_t(\bar{\mathcal{A}}_t) - P_t(\bar{\mathcal{A}}_i)], \quad (7)$$

where the expectation is taken over the prototypes. This approach assumes that the alignment for task  $t$ , which is computable, also applies to previous tasks  $i$  ( $< t$ ). The validity of this assumption is demonstrated experimentally. We refer to this mapping as *centroid prototype mapping*, with the detailed algorithm presented in Algorithm 1.

**Early Stopping for Adapter Merging:** As shown in Figure 4b, the alignment problem is not severe for tasks relatively close to the current one. Building on this observation, we introduce early stopping for adapter merging, which halts the merging process once the number of tasks exceeds a specified threshold.

While average merging is computationally efficient during inference, it can increase computational demands during training because adapters must be trained for each task. In Equation (5), as  $t$  grows, the difference between  $\theta_{t-1}$  and  $\theta_t$  becomes negligible, with the coefficient  $1/t$  approaching zero. This supports the effectiveness of early stopping, as further merging becomes redundant.

---

**Algorithm 1** Centroid prototype mapping on the  $t$ -th task.

---

**Input:** Merged adapters  $\bar{\mathcal{A}}_1, \dots, \bar{\mathcal{A}}_t$ , previous prototypes  $P_1(\bar{\mathcal{A}}_1), \dots, P_{t-1}(\bar{\mathcal{A}}_{t-1})$ .

**Output:** Prototypes aligned within the current subspace.

- 1:  $P_t(\bar{\mathcal{A}}_t) \leftarrow$  Calculate  $t$ -th task prototype with  $\bar{\mathcal{A}}_t$ .
  - 2:  $\triangleright$  Centroid prototype mapping
  - 3: **for**  $i = 1, \dots, t - 1$  **do**
  - 4:    $P_t(\bar{\mathcal{A}}_i) \leftarrow$  Calculate  $t$ -th task prototype with  $\bar{\mathcal{A}}_i$ .
  - 5:    $\Delta p \leftarrow \frac{1}{|\mathcal{Y}_t|} \sum_{c=1}^{|\mathcal{Y}_t|} (p_{t,c}(\bar{\mathcal{A}}_t) - p_{t,c}(\bar{\mathcal{A}}_i))$
  - 6:    $\Delta P \leftarrow [\Delta p \dots \Delta p] \in \mathbb{R}^{d \times |\mathcal{Y}_t|}$
  - 7:    $\hat{P}_i(\bar{\mathcal{A}}_t) \leftarrow P_i(\bar{\mathcal{A}}_i) + \Delta P$
  - 8: **end for**
  - 9: **return**  $\hat{P}_1(\bar{\mathcal{A}}_t), \dots, \hat{P}_{t-1}(\bar{\mathcal{A}}_t)$
- 

## 5. Experiments

We evaluate our method following the protocol defined in [56], assessing both performance and inference time. Additionally, we conduct an ablation study to validate the effectiveness of our approach.

### 5.1. Experimental Setup

**Datasets:** We evaluate our method on five benchmark datasets: CIFAR-100 [23] (CIFAR), CUB [45], ImageNet-R [16] (IN-R), ImageNet-A [15] (IN-A), and VTAB [53]. The details of each dataset are described in Appendix A. CIFAR-100 contains 100 classes, CUB, ImageNet-R, and ImageNet-A each contain 200 classes, and VTAB consists of 50 classes. For all datasets except VTAB, the class order is randomized for each seed. For VTAB, the class order is fixed. We divide these datasets into  $T$  tasks, using the notation “B- $m$  Inc- $n$ ”, where  $m$  is the initial number of classes, and  $n$  is the number of classes added incrementally per task. **Evaluation Metrics:** Following the standard protocol in CIL [33], we use two evaluation metrics: the average accuracy  $\bar{A}$  across all tasks and the accuracy  $A_T$  of the final task (final accuracy).

**Baselines:** We compare our method with several baselines and state-of-the-art methods. The baseline method is finetuning the pre-trained model for each task, referred to as Finetune. We also test finetuning only the adapter, referred to as Finetune Adapter. For comparison, we select CIL approaches using a pre-trained model: L2P [48], DualPrompt [47], CODA-Prompt [38], SimpleCIL [58], APER [58], and EASE [56]. Among these, SimpleCIL, APER, and EASE are prototype-based methods. SimpleCIL, a prototype-based CIL method without adapters, serves as the baseline. APER trains an adapter only for the first task and extracts feature vectors from the pre-trained model both with and without the adapter. EASE, by contrast, trains separate adapters for each task and individually extracts feature vectors from each adapter.

**Training Details:** We follow the training conditions used in [59]. For the pre-trained model, we use the ViT-B/16 model [12, 49], pre-trained on ImageNet-21K [34]. Adapter training is optimized using SGD with cosine annealing for the learning rate scheduler. The learning rate, batch size, and number of training epochs are set for each dataset, following the values specified in [59] (see Appendix B).

### 5.2. Main Results

Table 1 presents the average accuracy  $\bar{A}$  and final accuracy  $A_T$  for the five benchmark datasets. The results for the comparison methods are taken from [56], while the values for ACMap (ours) represent averages from five runs. Figure 5 shows the top-1 accuracy curve during CIL. The comparison methods include SimpleCIL, ADAM, and EASE, all of which are prototype-based methods. The values in the figure also represent averages from five runs for all methods. Additional results are provided in Appendix E.

ACMap performs comparably to or slightly better than EASE across all datasets, except VTAB B0 Inc10, and significantly outperforms APER on all datasets except CUB B0 Inc10. ACMap achieves notable improvements on domain-shifted datasets, such as IN-R, IN-A, and VTAB, compared to APER, which reuses the first adapter for all tasks. This suggests that ACMap’s approach to training and merging adapters enhances domain adaptation. However, on CUB B0 Inc10, adapter learning and merging did not improve performance, as even SimpleCIL, which lacks adapters, performs comparably to both APER and EASE.

In the VTAB B0 Inc10 experiment, EASE outperforms ACMap. This difference is likely due to the VTAB setup, which includes five datasets from distinct domains, with each task derived from a separate dataset. This setup allows EASE to use five distinct adapters, one for each dataset, whereas ACMap relies on a single adapter to learn from all five datasets. Therefore, when tasks span different domains, as in domain-incremental learning [43], task-specific subspaces may be more effective.

### 5.3. Inference Time

Additionally, a closer analysis of VTAB reveals that the dataset size for the fourth task is larger than that of the others, potentially causing overfitting on the fourth task. Consequently, as shown in Figure 5 (far right), model accuracy begins to decline from the fourth task, resulting in lower performance for ACMap than EASE.

Table 2 shows the inference time for task 40 of ImageNet-R B0 Inc5. The compared methods include SimpleCIL, APER, and EASE, with computational complexities of  $\mathcal{O}(1)$ ,  $\mathcal{O}(1)$ , and  $\mathcal{O}(T)$ , respectively, where  $T$  denotes the number of tasks. ACMap achieves a complexity of  $\mathcal{O}(1)$  because it uses only a single adapter for all tasks.

The results show that ACMap significantly outperforms

Table 1. Average accuracy  $\bar{A}$  and final accuracy  $A_T$ . CIFAR refers to CIFAR-100, and IN-R/A refers to ImageNet-R and ImageNet-A. Results for the comparison methods are taken from those reported in [56]. All evaluations are conducted in an exemplar-free setting. In our methods, IR denotes initial weight replacement.

Method	CIFAR B0 Inc5		CUB B0 Inc10		IN-R B0 Inc5		IN-A B0 Inc20		VTAB B0 Inc10	
	$\bar{A}$	$A_T$	$\bar{A}$	$A_T$	$\bar{A}$	$A_T$	$\bar{A}$	$A_T$	$\bar{A}$	$A_T$
Finetune	38.90	20.17	26.08	13.96	21.61	10.79	24.28	14.51	34.95	21.25
Finetune Adapter [5]	60.51	49.32	66.84	52.99	47.59	40.28	45.41	41.10	48.91	45.12
L2P [48]	85.94	79.93	67.05	56.25	66.53	59.22	49.39	14.71	77.11	77.10
DualPrompt [47]	87.87	81.15	77.47	66.54	63.31	55.22	53.71	41.67	83.36	81.23
CODA-Prompt [38]	89.11	81.96	84.00	73.37	64.42	55.08	53.54	42.73	83.90	83.02
SimpleCIL [58]	87.57	81.26	92.20	86.73	62.58	54.55	59.77	48.91	85.99	84.38
APER + Adapter [58]	90.65	85.15	92.21	86.73	72.35	64.33	60.47	49.37	85.95	84.35
EASE [56]	91.51	85.80	<b>92.23</b>	86.81	<b>78.31</b>	<b>70.58</b>	<b>65.34</b>	55.04	<b>93.61</b>	<b>93.55</b>
Ours w/o IR ( $L = 10$ )	91.53	87.35	91.74	<b>87.02</b>	76.47	69.88	63.95	54.63	90.28	86.25
Ours w/o IR ( $L = \infty$ )	91.54	87.35	91.74	86.96	76.56	70.08	64.00	54.67	90.28	86.25
Ours ( $L = 10$ )	92.01	87.73	91.59	86.61	77.10	70.25	65.14	56.04	91.21	87.56
Ours ( $L = \infty$ )	<b>92.04</b>	<b>87.81</b>	91.56	86.66	77.31	70.49	65.19	<b>56.19</b>	91.21	87.56

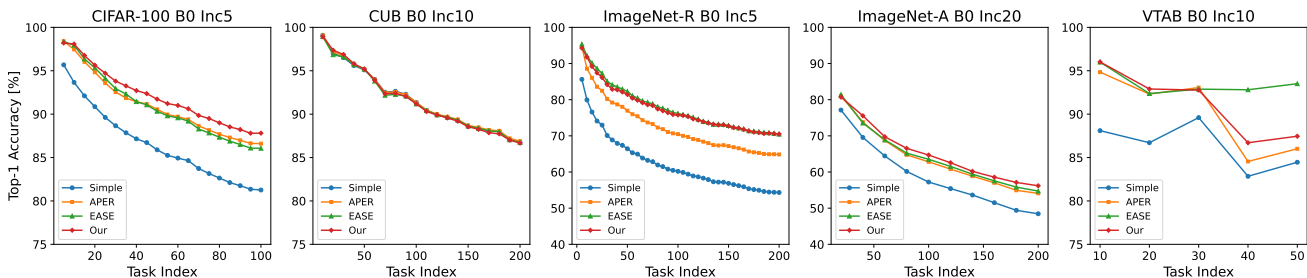


Figure 5. Top-1 accuracy curve during CIL, comparing prototype-based methods: SimpleCIL (denoted as Simple), APER, and EASE. Additional results are provided in Appendix E.

Table 2. Comparison of inference time for task 40 of IN-R B0 Inc5 among SimpleCIL, APER, EASE, and ACMap (ours). Time Ratio indicates how many times longer each comparative method’s inference time is compared to ACMap. ACMap achieves accuracy comparable to EASE while maintaining efficient inference.

Method	Time (s)	Time Ratio
SimpleCIL [58]	22.6	$\times 0.96$
APER [58]	44.1	$\times 1.88$
EASE [56]	916.5	$\times 39.0$
ACMap (ours)	23.5	-

EASE in terms of inference time, achieving a 39-fold speedup for 40 tasks. This speedup is particularly advantageous for real-world applications requiring long-term training and efficient inference.

Compared to SimpleCIL, ACMap achieves similar inference time while improving final top-1 accuracy by over 16%

Table 3. Ablation study for initial weight replacement (IR) and centroid prototype mapping (CM) with the symbol  $\checkmark$  indicating the method used. Both components contribute to the improvement of performance.

IR	CM	CIFAR B0 Inc5		IN-R B0 Inc5	
		$\bar{A}$	$A_T$	$\bar{A}$	$A_T$
		90.46	86.32	75.99	69.55
	$\checkmark$	91.53	87.35	76.47	69.88
$\checkmark$		91.07	86.85	76.56	69.80
$\checkmark$	$\checkmark$	<b>92.01</b>	<b>87.73</b>	<b>77.10</b>	<b>70.25</b>

(Table 1). Similarly, ACMap demonstrates comparable inference time to APER but surpasses it by over 6% in final top-1 accuracy. These results confirm ACMap’s success in balancing high accuracy and inference efficiency. Additional experiments on inference time are in Appendix C.

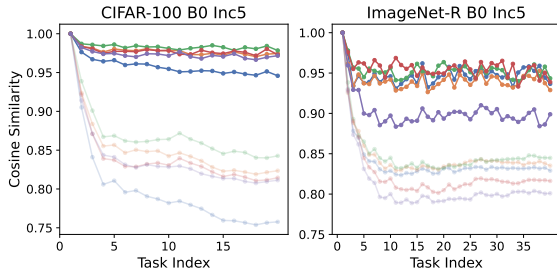


Figure 6. Cosine similarity curves of  $\text{Sim}(\hat{P}_1(\bar{A}_1), P_1(\bar{A}_t))$ , with solid lines showing the similarity between mapped and true prototypes, and semi-transparent lines between unmapped and true prototypes. The prototypes aligned through centroid prototype mapping move closer to the true prototype in subsequent tasks. Additional results are provided in Appendix D.1.

#### 5.4. Ablation Study

We conducted experiments on CIFAR-100 B0 Inc5 and ImageNet-R B0 Inc5 to conduct ablation studies.

**Centroid Prototype Mapping and Initial Weight Replacement:** We conducted ablation studies focusing on two key components: centroid prototype mapping (CM) and initial weight replacement (IR). The results of this study are presented in Table 3. These experiments fixed the early stopping parameter  $L$  at 10. The results indicate that both CM and IR contribute to performance improvement, emphasizing their role in enhancing the model’s overall effectiveness.

We further evaluated the effectiveness of centroid prototype mapping by examining how well the mapped prototypes  $\hat{P}_1(\bar{A}_t)$  align with the true prototypes  $P_1(\bar{A}_t)$  using cosine similarity. The true prototypes are computed using the validation datasets from previous tasks, which are unavailable in the CIL setting. The cosine similarity curve,  $\text{Sim}(\hat{P}_1(\bar{A}_t), P_1(\bar{A}_t))$ , as adapter merging progresses, is shown in Figure 6, where  $\text{Sim}(\cdot, \cdot)$  denotes cosine similarity. The solid line represents the cosine similarity between the mapped and true prototypes, while the semi-transparent line shows the similarity between the unmapped prototypes  $P_1(\bar{A}_1)$  and the true prototypes. The colors of the curves correspond to the classes from the first task. The results indicate that centroid prototype mapping effectively aligns the mapped prototypes with the true prototypes, as seen from the high cosine similarity values.

**Early Stopping Threshold:** We also evaluated the impact of the early stopping threshold,  $L$ , with results shown in Table 4. Since CIFAR-100 B0 Inc5 involves a total of 20 tasks, the results for  $L = 20$  are equivalent to those for  $L = \infty$ . The experiments show that increasing  $L$  generally

Table 4. Evaluation of the impact of the early stopping threshold  $L$ . By applying early stopping at around  $L = 10$ , unnecessary computations can be reduced without sacrificing model accuracy.

Threshold	CIFAR B0 Inc5		IN-R B0 Inc5	
	$\bar{A}$	$A_T$	$\bar{A}$	$A_T$
$L = 0$	91.07	86.85	76.56	69.80
$L = 5$	91.88	87.61	76.81	69.87
$L = 10$	92.00	87.76	77.09	70.25
$L = 20$	92.04	87.80	77.27	70.37
$L = \infty$	<b>92.04</b>	<b>87.80</b>	<b>77.31</b>	<b>70.49</b>

improves performance; however, the gains diminish as  $L$  increases. Furthermore, setting  $L = 10$  achieves performance comparable to  $L = \infty$ . This indicates that early stopping does not degrade performance and can prevent unnecessary computations without sacrificing model accuracy.

## 6. Conclusion

ACMap effectively addresses the challenges in CIL by retaining knowledge across tasks while scaling efficiently as the number of tasks increases. By merging task-specific adapters into a unified adapter, ACMap ensures that inference remains both efficient and consistent over time. The centroid prototype mapping mechanism refines task representations within a shared subspace, preserving accuracy as tasks accumulate. The experimental results across the five benchmarks demonstrate that ACMap not only matches the accuracy of state-of-the-art methods but also maintains constant inference time. This combination of competitive performance and scalability makes ACMap a promising approach for scenarios requiring efficient, scalable inference.

While ACMap demonstrates good performance, further refinements are needed when confronted with large domain gaps between tasks, such as those found in VTAB. A promising future direction is the concept of *adapter bank*. By selecting the most relevant adapters from a set of available options, the adapter bank approach could further improve ACMap’s performance across diverse scenarios.

## Acknowledgment

This work was supported by JSPS KAKENHI Grant Number JP23K24914

## References

- [1] Samuel Ainsworth, Jonathan Hayase, and Siddhartha Srinivasa. Git Re-Basin: Merging Models modulo Permutation Symmetries. In *International Conference on Learning Representations (ICLR)*, 2023. 4
- [2] Rahaf Aljundi, Punarjay Chakravarty, and Tinne Tuytelaars. Expert Gate: Lifelong Learning with a Network of Experts.



- In *Proceedings of the IEEE/CVF Conference on Computer Vision and Pattern Recognition (CVPR)*, pages 7120–7129, 2017. 2
- [3] Rahaf Aljundi, Min Lin, Baptiste Goujaud, and Yoshua Bengio. Gradient based sample selection for online continual learning. In *Neural Information Processing Systems (NeurIPS)*, pages 11816–11825, 2019. 1, 2
- [4] Arslan Chaudhry, Marc’Aurelio Ranzato, Marcus Rohrbach, and Mohamed Elhoseiny. Efficient Lifelong Learning with A-GEM. In *International Conference on Learning Representations (ICLR)*, 2019. 2
- [5] Shoufa Chen, Chongjian GE, Zhan Tong, Jiangliu Wang, Yibing Song, Jue Wang, and Ping Luo. AdaptFormer: Adapting Vision Transformers for Scalable Visual Recognition. In *Neural Information Processing Systems (NeurIPS)*, pages 16664–16678, 2022. 7
- [6] Prithviraj Dhar, Rajat Vikram Singh, Kuan-Chuan Peng, Ziyang Wu, and Rama Chellappa. Learning Without Memorizing. In *Proceedings of the IEEE/CVF Conference on Computer Vision and Pattern Recognition (CVPR)*, pages 5133–5141, 2019. 2
- [7] Alexey Dosovitskiy et al. An Image is Worth 16x16 Words: Transformers for Image Recognition at Scale. In *International Conference on Learning Representations (ICLR)*, 2021. 3
- [8] Arthur Douillard, Matthieu Cord, Charles Ollion, Thomas Robert, and Eduardo Valle. PODNet: Pooled Outputs Distillation for Small-Tasks Incremental Learning. In *European Conference on Computer Vision (ECCV)*, pages 86–102, 2020. 2
- [9] Arthur Douillard, Alexandre Ramé, Guillaume Couairon, and Matthieu Cord. DyTox: Transformers for Continual Learning with DYNAMIC TOKEN EXPANSION. In *Proceedings of the IEEE/CVF Conference on Computer Vision and Pattern Recognition (CVPR)*, pages 9275–9285, 2022. 2
- [10] Robert M. French. Catastrophic forgetting in connectionist networks. *Trends in Cognitive Sciences*, pages 128–135, 1999. 1, 2
- [11] Spyros Gidaris and Nikos Komodakis. Dynamic Few-Shot Visual Learning Without Forgetting. In *Proceedings of the IEEE/CVF Conference on Computer Vision and Pattern Recognition (CVPR)*, pages 4367–4375, 2018. 2, 3
- [12] google. <https://huggingface.co/google/vit-base-patch16-224-in21k>, 2021. 6, 2
- [13] Xu Han et al. Pre-trained models: Past, present and future. *AI Open*, pages 225–250, 2021. 2
- [14] Zeyu Han, Chao Gao, Jinyang Liu, Jeff Zhang, and Sai Qian Zhang. Parameter-Efficient Fine-Tuning for Large Models: A Comprehensive Survey. *Transactions on Machine Learning Research*, 2024. 2
- [15] Dan Hendrycks, Kevin Zhao, Steven Basart, Jacob Steinhardt, and Dawn Song. Natural Adversarial Examples. In *Proceedings of the IEEE/CVF Conference on Computer Vision and Pattern Recognition (CVPR)*, pages 15262–15271, 2021. 6, 1
- [16] Dan Hendrycks et al. The Many Faces of Robustness: A Critical Analysis of Out-of-Distribution Generalization. In *International Conference on Computer Vision (ICCV)*, pages 8320–8329, 2021. 6, 1
- [17] Geoffrey Hinton, Oriol Vinyals, and Jeffrey Dean. Distilling the Knowledge in a Neural Network. In *NIPS Deep Learning and Representation Learning Workshop*, 2015. 2
- [18] Edward J Hu, yelong shen, Phillip Wallis, Zeyuan Allen-Zhu, Yuanzhi Li, Shean Wang, Lu Wang, and Weizhu Chen. LoRA: Low-Rank Adaptation of Large Language Models. In *International Conference on Learning Representations (ICLR)*, 2022. 2
- [19] Xinting Hu, Kaihua Tang, Chunyan Miao, Xian-Sheng Hua, and Hanwang Zhang. Distilling Causal Effect of Data in Class-Incremental Learning. In *Proceedings of the IEEE/CVF Conference on Computer Vision and Pattern Recognition (CVPR)*, pages 3957–3966, 2021. 2
- [20] Gabriel Ilharco, Marco Tulio Ribeiro, Mitchell Wortsman, Ludwig Schmidt, Hannaneh Hajishirzi, and Ali Farhadi. Editing models with task arithmetic. In *International Conference on Learning Representations (ICLR)*, 2023. 4
- [21] Menglin Jia, Luming Tang, Bor-Chun Chen, Claire Cardie, Serge Belongie, Bharath Hariharan, and Ser-Nam Lim. Visual Prompt Tuning. In *European Conference on Computer Vision (ECCV)*, pages 709–727, 2022. 1, 2
- [22] James Kirkpatrick, Razvan Pascanu, Neil Rabinowitz, Joel Veness, Guillaume Desjardins, Andrei A. Rusu, Kieran Milan, John Quan, Tiago Ramalho, Agnieszka Grabska-Barwinska, Demis Hassabis, Claudia Clopath, Dharshan Kumaran, and Raia Hadsell. Overcoming catastrophic forgetting in neural networks. *National Academy of Sciences*, pages 3521–3526, 2017. 2
- [23] Alex Krizhevsky. Learning Multiple Layers of Features from Tiny Images. *University of Toronto*, 2009. 6, 1
- [24] Weishi Li, Yong Peng, Miao Zhang, Liang Ding, Han Hu, and Li Shen. Deep Model Fusion: A Survey, 2023. 4
- [25] Yixuan Li, Jason Yosinski, Jeff Clune, Hod Lipson, and John Hopcroft. Convergent Learning: Do different neural networks learn the same representations? In *Proceedings of the 1st International Workshop on Feature Extraction: Modern Questions and Challenges at NIPS 2015*, pages 196–212, 2015. 4
- [26] Zhizhong Li and Derek Hoiem. Learning without Forgetting. *IEEE Transactions on Pattern Analysis and Machine Intelligence*, pages 2935–2947, 2018. 2
- [27] Yaoyao Liu, Bernt Schiele, and Qianru Sun. RMM: Reinforced Memory Management for Class-Incremental Learning. In *Neural Information Processing Systems (NeurIPS)*, pages 3478–3490, 2021. 2
- [28] David Lopez-Paz and Marc’Aurelio Ranzato. Gradient episodic memory for continual learning. In *Neural Information Processing Systems (NeurIPS)*, pages 6470–6479, 2017. 1, 2
- [29] Michael S Matena and Colin A Raffel. Merging Models with Fisher-Weighted Averaging. In *Neural Information Processing Systems (NeurIPS)*, pages 17703–17716, 2022. 4
- [30] Oleksiy Ostapenko, Mihai Puscas, Tassilo Klein, Patrick Jah-nichen, and Moin Nabi. Learning to Remember: A Synaptic Plasticity Driven Framework for Continual Learning. In *Proceedings of the IEEE/CVF Conference on Computer Vision*

- and Pattern Recognition (CVPR), pages 11313–11321, 2019. 2
- [31] Jonas Pfeiffer, Aishwarya Kamath, Andreas Rücklé, Kyunghyun Cho, and Iryna Gurevych. AdapterFusion: Non-Destructive Task Composition for Transfer Learning. In *European Chapter of the Association for Computational Linguistics*, pages 487–503, 2021. 1
- [32] Quang Pham, Chenghao Liu, and Steven Hoi. DualNet: Continual Learning, Fast and Slow. In *Neural Information Processing Systems (NeurIPS)*, pages 16131–16144, 2021. 2
- [33] Sylvestre-Alvise Rebuffi, Alexander Kolesnikov, Georg Sperl, and Christoph H. Lampert. iCaRL: Incremental Classifier and Representation Learning. In *Proceedings of the IEEE/CVF Conference on Computer Vision and Pattern Recognition (CVPR)*, pages 5533–5542, 2017. 1, 2, 6
- [34] Tal Ridnik, Emanuel Ben-Baruch, Asaf Noy, and Lihi Zelnik. ImageNet-21K Pretraining for the Masses. In *Proceedings of Neural Information Processing Systems Track on Datasets and Benchmarks*, 2021. 6, 1
- [35] Hanul Shin, Jung Kwon Lee, Jaehong Kim, and Jiwon Kim. Continual learning with deep generative replay. In *Neural Information Processing Systems (NeurIPS)*, pages 2994–3003, 2017. 1, 2
- [36] Reza Shokri and Vitaly Shmatikov. Privacy-Preserving Deep Learning. In *ACM SIGSAC Conference on Computer and Communications Security*, pages 1310–1321, 2015. 1
- [37] Christian Simon, Piotr Koniusz, and Mehrtash Harandi. On Learning the Geodesic Path for Incremental Learning. In *Proceedings of the IEEE/CVF Conference on Computer Vision and Pattern Recognition (CVPR)*, pages 1591–1600, 2021. 2
- [38] J. Smith, L. Karlinsky, V. Gutta, P. Cascante-Bonilla, D. Kim, A. Arbellet, R. Panda, R. Feris, and Z. Kira. CODA-Prompt: COntinual Decomposed Attention-Based Prompting for Rehearsal-Free Continual Learning. In *Proceedings of the IEEE/CVF Conference on Computer Vision and Pattern Recognition (CVPR)*, pages 11909–11919, 2023. 1, 6, 7
- [39] Jake Snell, Kevin Swersky, and Richard Zemel. Prototypical networks for few-shot learning. In *Neural Information Processing Systems (NeurIPS)*, pages 4080–4090, 2017. 2
- [40] Norman Tatro, Pin-Yu Chen, Payel Das, Igor Melnyk, Prasanna Sattigeri, and Rongjie Lai. Optimizing Mode Connectivity via Neuron Alignment. In *Neural Information Processing Systems (NeurIPS)*, pages 15300–15311, 2020. 4
- [41] Sebastian Thrun. Is Learning The n-th Thing Any Easier Than Learning The First? In *Neural Information Processing Systems (NeurIPS)*, pages 640–646, 1995. 1
- [42] Rishabh Tiwari, Krishnateja Killamsetty, Rishabh Iyer, and Pradeep Shenoy. GCR: Gradient Coreset Based Replay Buffer Selection for Continual Learning. In *Proceedings of the IEEE/CVF Conference on Computer Vision and Pattern Recognition (CVPR)*, pages 99–108, 2022. 2
- [43] Guido van de Ven, Tinne Tuytelaars, and Andreas Tolias. Three types of incremental learning. *Nature Machine Intelligence*, pages 1–13, 2022. 6
- [44] Ashish Vaswani, Noam Shazeer, Niki Parmar, Jakob Uszkoreit, Llion Jones, Aidan N. Gomez, Łukasz Kaiser, and Illia Polosukhin. Attention is all you need. In *Neural Information Processing Systems (NeurIPS)*, pages 6000–6010, 2017. 3
- [45] Catherine Wah, Steve Branson, Peter Welinder, Pietro Perona, and Serge Belongie. The Caltech-UCSD Birds-200-2011 Dataset. Technical report, California Institute of Technology, 2011. 6, 1
- [46] Fu-Yun Wang, Da-Wei Zhou, Han-Jia Ye, and De-Chuan Zhan. FOSTER: Feature Boosting and Compression for Class-Incremental Learning. In *European Conference on Computer Vision (ECCV)*, pages 398–414, 2022. 1, 2
- [47] Zifeng Wang et al. DualPrompt: Complementary Prompting for Rehearsal-Free Continual Learning. In *European Conference on Computer Vision (ECCV)*, pages 631–648, 2022. 1, 6, 7
- [48] Zifeng Wang et al. Learning to Prompt for Continual Learning. In *Proceedings of the IEEE/CVF Conference on Computer Vision and Pattern Recognition (CVPR)*, pages 139–149, 2022. 1, 6, 7
- [49] Ross Wightman. <https://github.com/huggingface/pytorch-image-models>, 2019. 6
- [50] Mitchell Wortsman et al. Model soups: averaging weights of multiple fine-tuned models improves accuracy without increasing inference time. In *International Conference on Machine Learning (ICML)*, pages 23965–23998, 2022. 4
- [51] Prateek Yadav, Derek Tam, Leshem Choshen, Colin A Raffel, and Mohit Bansal. TIES-Merging: Resolving Interference When Merging Models. In *Neural Information Processing Systems (NeurIPS)*, pages 7093–7115, 2023. 4
- [52] S. Yan, J. Xie, and X. He. DER: Dynamically Expandable Representation for Class Incremental Learning. In *Proceedings of the IEEE/CVF Conference on Computer Vision and Pattern Recognition (CVPR)*, pages 3013–3022, 2021. 1, 2
- [53] Xiaohua Zhai et al. A Large-scale Study of Representation Learning with the Visual Task Adaptation Benchmark, 2020. 6, 1
- [54] Da-Wei Zhou, Qi-Wei Wang, Han-Jia Ye, and De-Chuan Zhan. A Model or 603 Exemplars: Towards Memory-Efficient Class-Incremental Learning. In *International Conference on Learning Representations (ICLR)*, 2023. 1, 2
- [55] Da-Wei Zhou, Hai-Long Sun, Jingyi Ning, Han-Jia Ye, and De-Chuan Zhan. Continual learning with pre-trained models: A survey. In *International Joint Conference on Artificial Intelligence*, pages 8363–8371, 2024. 1, 2
- [56] Da-Wei Zhou, Hai-Long Sun, Han-Jia Ye, and De-Chuan Zhan. Expandable Subspace Ensemble for Pre-Trained Model-Based Class-Incremental Learning. In *Proceedings of the IEEE/CVF Conference on Computer Vision and Pattern Recognition (CVPR)*, pages 23554–23564, 2024. 1, 2, 3, 6, 7
- [57] Da-Wei Zhou, Qi-Wei Wang, Zhi-Hong Qi, Han-Jia Ye, De-Chuan Zhan, and Ziwei Liu. Class-Incremental Learning: A Survey. *IEEE Transactions on Pattern Analysis and Machine Intelligence*, pages 1–20, 2024. 2
- [58] Da-Wei Zhou, Han-Jia Ye, De-Chuan Zhan, and Ziwei Liu. Revisiting Class-Incremental Learning with Pre-Trained Models: Generalizability and Adaptivity are All You Need. *International Journal of Computer Vision*, 2024. 1, 2, 3, 6, 7

- [59] Da-Wei Zhou, Hai-Long Sun, Han-Jia Ye, and De-Chuan Zhan. <https://github.com/sun-hailong/CVPR24-Ease>, 2024. 6, 2

# Adapter Merging with Centroid Prototype Mapping for Scalable Class-Incremental Learning

## Supplementary Material

### A. Dataset Details

This section describes the benchmark datasets used in the experiments. Figure A illustrates example images from CIFAR-100, CUB, ImageNet-R, ImageNet-A, and VTAB. Since the pre-trained model is trained on ImageNet-21K [34], ImageNet is excluded as a benchmark dataset.

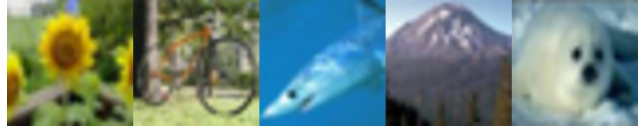
**CIFAR-100:** CIFAR-100 [23] contains 100 classes and is widely used for image classification. CIFAR-100 serves as a standard benchmark in class-incremental learning (CIL) due to its small-sized images and diverse object categories. CIFAR-100 is particularly suitable for evaluating basic performance in simpler CIL settings.

**CUB:** Caltech-UCSD Birds 200 (CUB) [45] contains 200 classes and is a benchmark for fine-grained classification. Its primary challenge is distinguishing visually similar categories, such as bird species, requiring detailed feature extraction and handling high intra-class variation. This challenge makes it a compelling dataset for evaluating CIL performance in fine-grained settings.

**ImageNet-R:** ImageNet-R [16], a variant of the ImageNet dataset, contains images with 200 classes from diverse domains, such as art, cartoons, and paintings. This dataset evaluates a model’s ability to generalize across domains and is particularly valuable for evaluating the domain generalization capabilities of models trained on ImageNet. In CIL settings, ImageNet-R measures adaptability to new domains introduced incrementally.

**ImageNet-A:** ImageNet-A [15], a subset of ImageNet, contains 200 classes with adversarial or out-of-distribution examples that models often misclassify. This dataset, designed to challenge models trained on standard ImageNet, includes images that are particularly difficult to classify. ImageNet-A evaluates robustness to adversarial attacks and generalization to unseen data, establishing itself as a critical benchmark in CIL settings.

**VTAB:** Visual Task Adaptation Benchmark (VTAB) [53] contains a collection of datasets designed to evaluate a model’s adaptability to diverse tasks. This benchmark primarily serves to evaluate transfer learning and domain adaptation capabilities. Following the protocol in [56], this study constructs a 50-class dataset by selecting five subsets



(a) CIFAR-100.



(b) CUB.



(c) ImageNet-R.



(d) ImageNet-A.



(e) VTAB.

Figure A. Example images from (a) CIFAR-100, (b) CUB, (c) ImageNet-R, (d) ImageNet-A, and (e) VTAB.

from VTAB: Resisc45 (classes 1-10), Describable Textures Dataset (DTD) (classes 11-20), Oxford IIIT Pet dataset (classes 21-30), EuroSAT (classes 31-40), and 102 Category Flower Dataset (classes 41-50).

### B. Implementation Details

This section provides details of the implementation setup. The batch size, learning rate, weight decay, and number of training epochs for each dataset are shown in Table A. Each experiment was repeated five times, with the seeds set to 1993, 1994, 1995, 1996, and 1997. The experiments were conducted on a single NVIDIA RTX A5000, with PyTorch



Table A. Details of the training settings for each dataset, based on the configurations provided in [59].

dataset	batch size	learning rate	weight decay	epochs
CIFAR-100	48	$2.5 \times 10^{-2}$	$5.0 \times 10^{-4}$	20
CUB	32	$8.0 \times 10^{-3}$	$5.0 \times 10^{-4}$	20
ImageNet-R	16	$5.0 \times 10^{-2}$	$5.0 \times 10^{-3}$	20
ImageNet-A	32	$5.0 \times 10^{-2}$	$5.0 \times 10^{-3}$	20
VTAB	16	$3.0 \times 10^{-2}$	$5.0 \times 10^{-3}$	45

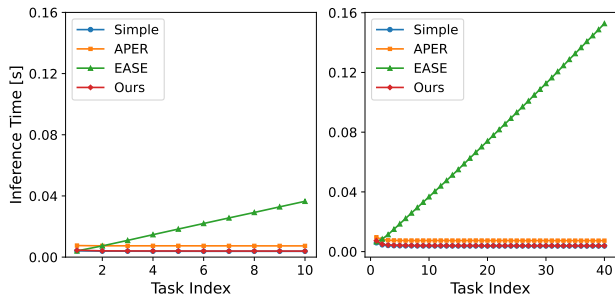


Figure B. Inference time curves per instance on ImageNet-R B0 Inc20 (left) and B0 Inc5 (right). Simple CIL, APER, and ACMap (ours) maintain a consistent inference time regardless of the increase in task count, while EASE exhibits a linear increase in inference time.

for model training and inference.

**Model Architecture:** The backbone model used in the experiments is ViT-B/16 [12], with an embedding dimension of 768, a patch size of 16, and 12 transformer blocks. The multi-head attention employs 12 attention heads. The adapter is configured with a bottleneck dimension of 64, a dropout rate of 0.1, and an up-projection scale of 0.1.

**Preprocessing:** The preprocessing pipeline involves random cropping with scales ranging from 0.05 to 1.0 and aspect ratios between 3:4 and 4:3, followed by horizontal flipping with a probability of 0.5. The images are resized to  $224 \times 224$  and normalized to the range [0, 1].

### C. Inference Time Comparison

This section presents additional inference time results comparing ACMap (ours) and the compared methods: SimpleCIL [58], APER [58], and EASE [56].at of EASE. Moreover, while having a similar inference time as SimpleCIL and APER, our method outperforms them in terms of accuracy.

## D. Additional Experiments on Centroid Prototype Mapping

This section presents additional experimental results to demonstrate the effectiveness of centroid prototype mapping and analyze the test-error landscape for adapter merging on datasets not covered in the main paper, including results from the main paper for comparison.

### D.1. Centroid Prototype Mapping

Figure C presents additional experiments for centroid prototype mapping. These experiments evaluate the alignment between the mapped and true prototypes by calculating cosine similarities. The solid line represents the cosine similarity between the mapped and true prototypes, while the semi-transparent line shows the cosine similarity between the unmapped and true prototypes. The colors of the curves correspond to the classes from the first task.

Across all datasets, the solid lines demonstrate consistently higher cosine similarity compared to the semi-transparent lines. This result confirms that centroid prototype mapping effectively aligns the prototypes from the previous tasks with the true prototypes in the current subspace. Interestingly, for CUB, a fine-grained classification dataset, the semi-transparent lines already exhibit high cosine similarity. This observation suggests that in fine-grained classification tasks, adapters and adapter merging are not necessarily required, and their benefits may be limited. As shown in Table 1 of the main paper, SimpleCIL, which does not use adapters, exhibits accuracy comparable to ACMap, APER, and EASE.

### D.2. Landscape Analysis for Adapter Merging

Figure D presents the test-error landscapes of three successive adapters,  $\theta_{t-1}$ ,  $\theta_t$ ,  $\theta_{t+1}$  through the linear interpolation on the datasets not covered in the main paper. For CIFAR-100 B0 Inc20 and VTAB B0 Inc10, only the result for  $\theta_2$ ,  $\theta_3$ ,  $\theta_4$  is presented because the task count is limited to five, meaning  $\theta_6$ ,  $\theta_7$  are not available.

Across all datasets except VTAB, these results indicate that ACMap promotes the formation of low-loss basins (red regions), demonstrating that the conditions for successful adapter merging are satisfied. Precisely speaking, for CUB,

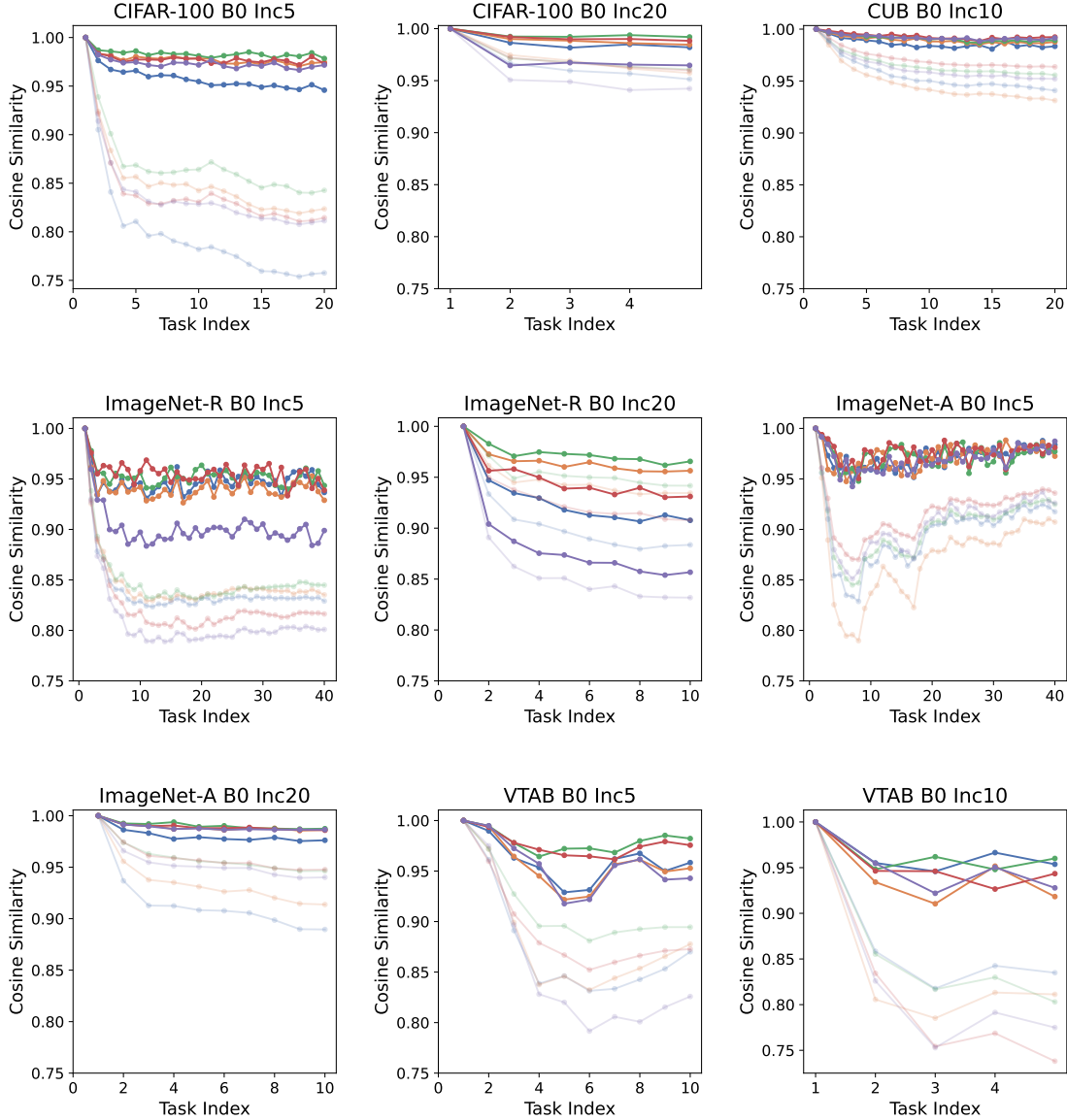


Figure C. Cosine similarity curves of  $\text{Sim}(\hat{\mathbf{P}}_1(\bar{\mathcal{A}}_1), \mathbf{P}_1(\bar{\mathcal{A}}_t))$ , with solid lines showing the similarity between mapped and true prototypes, and semi-transparent lines between unmapped and true prototypes, illustrating the alignment achieved by centroid prototype mapping.

rather than forming low-loss basins, the results indicate the formation of flat landscapes. This result suggests that adapter merging is not necessarily required to achieve CIL in CUB, as discussed in Appendix D.1.

Moreover, as illustrated in Figure D (g), (h), low-loss basins are not evident for VTAB. As discussed in Section 5.2, adapter merging does not consistently succeed when tasks exhibit significant domain gaps. Additionally, as mentioned in the main paper, the dataset size for the fourth task in VTAB is larger than that of the others, which may lead to overfitting on the fourth task. The low test-error rate

(red) observed around  $\theta_4$  in Figure D (h) supports this hypothesis. This hypothesis is also supported by the VTAB B0 Inc10 result in Figure 5 of the main paper, where ACMap demonstrates a significant decline in accuracy starting from the fourth task.

## E. Top-1 Accuracy Comparison

Figure E presents the top-1 accuracy curves for all experiments conducted in this study, comparing ACMap (ours) with SimpleCIL, APER, and EASE. The graphs include the

results from the main paper for comparison and reference.

The experimental results are consistent with those reported in the main paper, showing that ACMap outperforms or achieves comparable accuracy to the other methods across all datasets except for VTAB. While ACMap demonstrates comparable accuracy to EASE, it is important to recall, as discussed in Appendix C, that ACMap is T-times faster than EASE. This fact highlights that ACMap achieves state-of-the-art accuracy and ensures constant inference time, making it suitable for scalable CIL.

When the number of tasks in VTAB reaches 4 in Figure E (bottom middle and right), ACMap exhibits a significant drop in accuracy, leading to lower performance compared to EASE. As discussed in Appendix D.2, this decline is likely caused by the data imbalance, which may result in overfitting. EASE, on the other hand, avoids such issues by maintaining separate adapters for each task, though this comes at the expense of increased inference time.

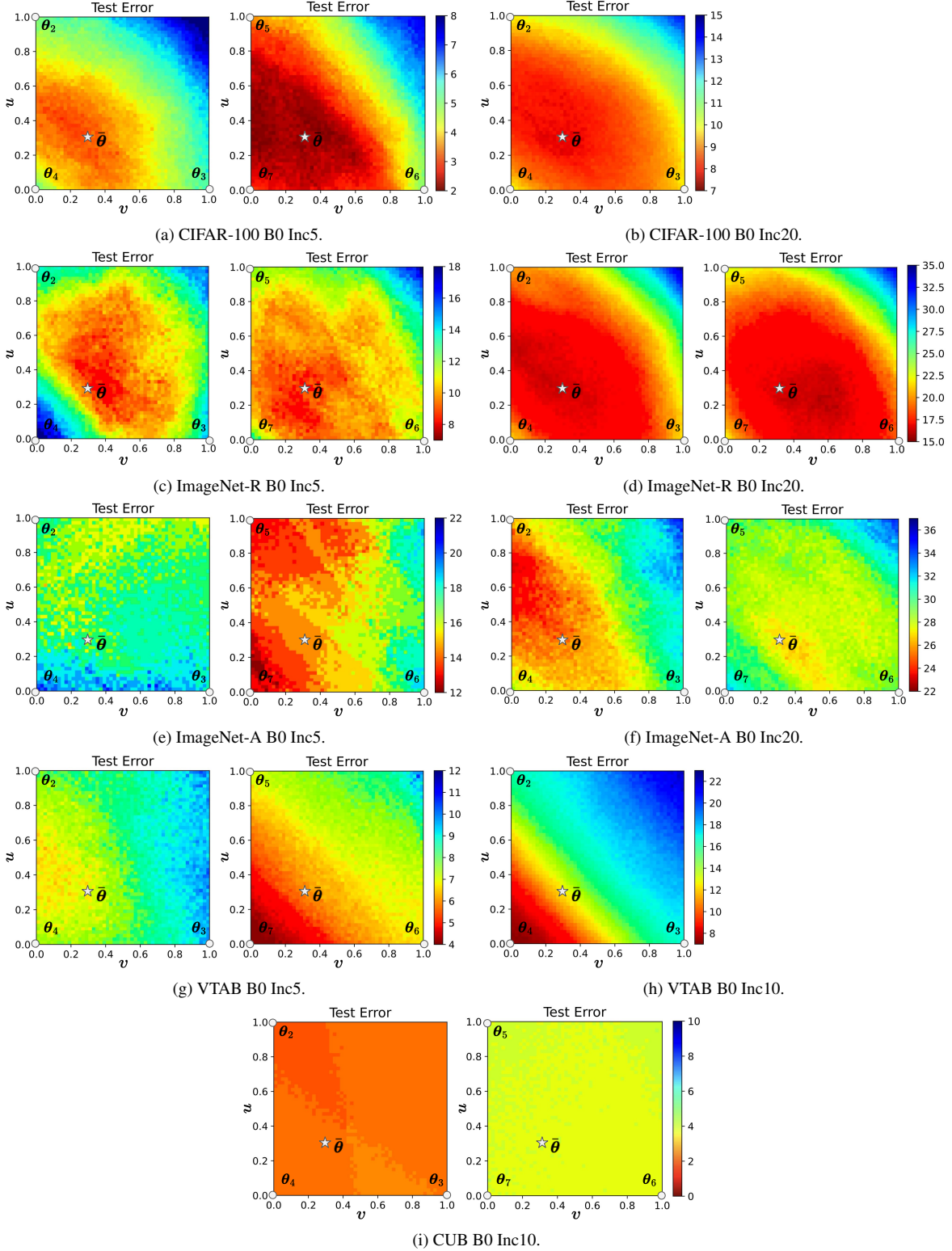


Figure D. Additional results for visualization of the test error on CIFAR-100, CUB, ImageNet-R, ImageNet-A, and VTAB using linearly interpolated adapter weights  $\theta = u\theta_{t-1} + v\theta_t + (1-u-v)\theta_{t+1}$ , ( $0 \leq u, v \leq 1$ ) across three consecutive adapter weights  $\theta_{t-1}, \theta_t, \theta_{t+1}$ . For CIFAR-100 B0 Inc20 and VTAB B0 Inc10, only the result for  $\theta_2, \theta_3, \theta_4$  is presented because the task count is limited to five, meaning  $\theta_6, \theta_7$  are not available.



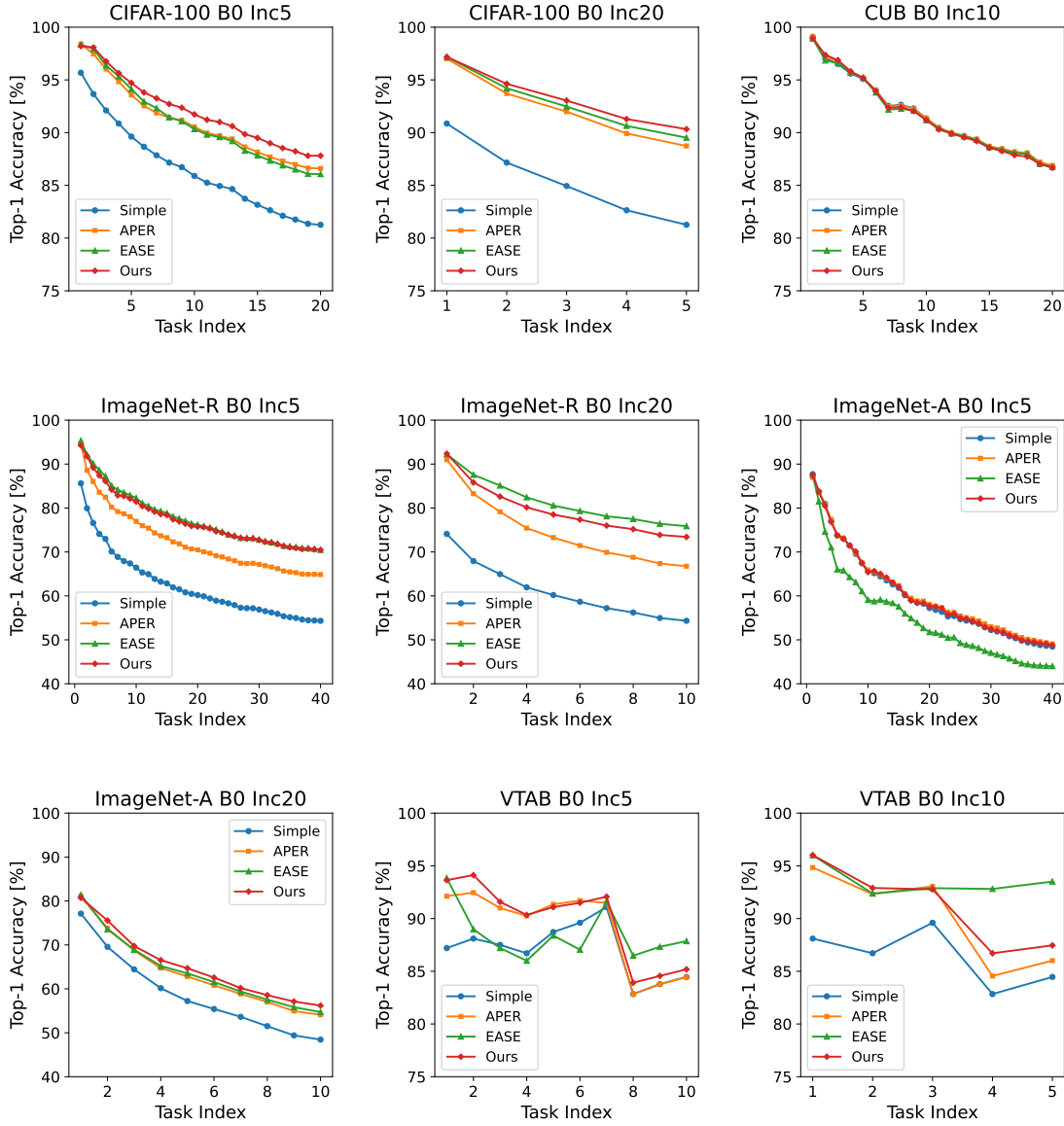


Figure E. Top-1 accuracy curves during CIL for all experiments conducted, comparing ACMap (ours) with SimpleCIL, APER, and EASE. These graphs include the results from the main paper for comparison and reference.